

WHAT DOES A SUBMILLIMETER GALAXY SELECTION ACTUALLY SELECT? THE DEPENDENCE OF SUBMILLIMETER FLUX DENSITY ON STAR FORMATION RATE AND DUST MASS

CHRISTOPHER C. HAYWARD^{1,2}, DUŠAN KEREŠ^{1,3,4}, PATRIK JONSSON¹,
DESIKA NARAYANAN^{1,5,6}, T. J. COX⁷, AND LARS HERNQUIST¹

Draft version December 2, 2024

ABSTRACT

We perform 3-D dust radiative transfer (RT) calculations on hydrodynamic simulations of isolated and merging disk galaxies in order to quantitatively study the dependence of observed-frame submillimeter (submm) flux density on galaxy properties. We find that submm flux density and star formation rate (SFR) are related in dramatically different ways for quiescently star-forming galaxies and starbursts. Because the stars formed in the merger-induced starburst do not dominate the bolometric luminosity and the rapid drop in dust mass and more compact geometry cause a sharp increase in dust temperature during the burst, starbursts are very inefficient at boosting submm flux density (e.g., a $\gtrsim 16x$ boost in SFR yields a $\lesssim 2x$ boost in submm flux density). Moreover, the ratio of submm flux density to SFR differs significantly between the two modes; thus one cannot assume that the galaxies with highest submm flux density are necessarily those with the highest bolometric luminosity or SFR. These results have important consequences for the submillimeter-selected galaxy (SMG) population. Among them are: 1. The SMG population is heterogeneous. In addition to the canonical scenario of merger-driven starbursts, there is a galaxy pair contribution in which two disks undergoing a major merger but not yet strongly interacting are blended into one submm source because of the large ($\gtrsim 15''$, or ~ 130 kpc at $z = 2$) beam of submm bolometers. 2. SMGs must be very massive ($M_{\star} \gtrsim 6 \times 10^{10} M_{\odot}$). 3. The infall phase makes the SMG duty cycle a factor of a few greater than what is expected for a merger-driven starburst. Finally, we provide fitting functions for SCUBA and AzTEC submm flux densities as a function of SFR and dust mass and bolometric luminosity and dust mass; these should be useful for calculating submm flux density in semi-analytic models and cosmological simulations when performing full RT is computationally not feasible.

Subject headings: galaxies: high-redshift — galaxies: interactions — galaxies: starburst — hydrodynamics — radiative transfer — submillimeter: galaxies.

1. INTRODUCTION

Submillimeter-selected galaxies (SMGs; Smail et al. 1997; Barger et al. 1998; Hughes et al. 1998; Eales et al. 1999; see Blain et al. 2002 for a review) are extremely luminous (bolometric luminosity $L_{\text{bol}} \sim 10^{12} - 10^{13} L_{\odot}$; e.g., Kovács et al. 2006), high-redshift (Chapman et al. 2005) galaxies powered primarily by star formation rather than AGN (Alexander et al. 2005a,b, 2008; Valiante et al. 2007; Menéndez-Delmestre et al. 2007, 2009; Pope et al. 2008; Younger et al. 2008, 2009b). Because of their high dust content, SMGs emit almost all of their luminosity in the IR. As the name suggests, a galaxy is defined as an SMG if it is detected in the submm (historically, 850 μm flux density $S_{850} \gtrsim 3 - 5$ mJy; the nature of the population is sensitive to the adopted flux density cut), which re-

quires $L_{\text{IR}} \gtrsim 10^{12} L_{\odot}$ (Kovács et al. 2006; Coppin et al. 2008), so SMGs are typically ultra-luminous infrared galaxies (ULIRGs). Locally, ULIRGs are almost exclusively merging galaxies (Sanders & Mirabel 1996; Lonsdale et al. 2006), so one might expect that at least some SMGs are also merging galaxies. Indeed, many observations support a merger origin for SMGs (e.g., Ivison et al. 2002, 2007; Chapman et al. 2003; Neri et al. 2003; Smail et al. 2004; Swinbank et al. 2004; Greve et al. 2005; Tacconi et al. 2006, 2008; Bouché et al. 2007; Biggs & Ivison 2008; Capak et al. 2008; Younger et al. 2008, 2010; Iono et al. 2009; Engel et al. 2010). Furthermore, in Narayanan et al. (2010b, hereafter N10) we combined hydrodynamic simulations and radiative transfer (RT) calculations to show that major mergers can reproduce the full range of submm flux densities and typical UV-mm spectral energy distribution (SED) of SMGs (cf. Chakrabarti et al. 2008). Semi-analytic models also predict that the SMG population is dominated by merger-induced starbursts rather than quiescent star formation (Baugh et al. 2005; Fontanot et al. 2007; Swinbank et al. 2008; Lo Faro et al. 2009; Fontanot & Monaco 2010; Gonzalez et al. 2010; but cf. Granato et al. 2004).

However, because of the much greater rate of gas supply onto galaxies at high redshift (e.g., Kereš et al. 2005; Dekel et al. 2009), gas fractions (Erb et al. 2006;

¹ Harvard-Smithsonian Center for Astrophysics, 60 Garden Street, Cambridge, MA 02138, USA

² chayward@cfa.harvard.edu

³ Department of Astronomy and Theoretical Astrophysics Center, University of California Berkeley, Berkeley, CA 94720, USA

⁴ Hubble Fellow

⁵ Steward Observatory, Department of Astronomy, University of Arizona, 933 North Cherry Avenue, Tucson, AZ 85721, USA

⁶ Bart J. Bok Fellow

⁷ Carnegie Observatories, 813 Santa Barbara Street, Pasadena, CA 91101, USA

Tacconi et al. 2006, 2010; Daddi et al. 2010) and star formation rates (Daddi et al. 2007; Noeske et al. 2007a,b) of galaxies at fixed galaxy mass increase rapidly with redshift. Thus, at $z \sim 2 - 3$ even a “normal” star-forming galaxy can reach ULIRG luminosities (e.g., Hopkins et al. 2008c, 2010; Daddi et al. 2005, 2007; Dannerbauer et al. 2009). Furthermore, roughly estimating submm counts using estimates of high-redshift major merger rates and the short duty cycle of merger-induced starbursts suggests that there may not be enough major mergers to account for the SMG population (Davé et al. 2010). This motivates the view that, instead, typical SMGs may be massive, gas-rich disks quiescently forming stars and fueled by continuous gas supply from mergers and smooth accretion (Genzel et al. 2003; Davé et al. 2010).

The mode of star formation responsible for the majority of the SMG population is still a matter of debate, as it is difficult to discriminate between the two scenarios given the currently available data. A better understanding of the submm galaxy selection can clarify the nature of the SMG population.

Since SMGs have redshifts $z \sim 1 - 4$ (Chapman et al. 2005; Younger et al. 2007, 2008; Capak et al. 2008; Greve et al. 2008; Schinnerer et al. 2008; Daddi et al. 2009a,b; Knudsen et al. 2010), the observed submm flux density traces rest-frame $\sim 150 - 400 \mu\text{m}$, longward of the peak of the IR SED. Thus the observed submm flux density is sensitive to both the total IR luminosity and the “dust temperature”⁸ of the SED, which depend on the luminosity from stars and AGN absorbed by the dust and the mass, composition, and spatial distribution of the dust. Galaxies do not have identical SED shapes, so the dependence on dust temperature implies that galaxies with the highest submm flux density are not necessarily those with the highest bolometric luminosity. Furthermore, because star formation histories are more complicated than an instantaneous burst, the luminosity and instantaneous SFR are not necessarily linearly proportional. Thus the relationship between submm flux density and SFR is potentially more complicated than the relationship between submm flux density and bolometric luminosity. We therefore cannot say *a priori* that the galaxies with the highest submm flux densities are the most rapidly star-forming or most luminous bolometrically. Indeed, it has already been observationally demonstrated that submm selection does not select all the brightest galaxies in a given volume, as there are galaxies with luminosities and redshifts comparable to those of SMGs that are undetected in the submm because of their relatively hot SEDs (Chapman et al. 2004; Chapman et al. 2010; Casey et al. 2009; Casey et al. 2010; Hwang et al. 2010; Magdis et al. 2010; Magnelli et al. 2010). A submm galaxy selection is clearly biased toward cold galaxies; however, the details of the selection bias are yet to be understood.

Despite the basic physical reasons that one does not

⁸ As is convention, we will use the term “dust temperature” to denote the temperature derived from a single-temperature modified blackbody fit to the SED. This is simply a parameterization of the SED shape rather than a physical temperature. In our simulations dust grains have a continuum of temperatures, depending on both grain size and the local radiation field heating the dust.

expect a simple relation between submm flux density and SFR, a linear relation between submm flux and SFR has been used explicitly (and, even more frequently, implicitly) to infer SFR from observed submm flux densities (e.g., Chapman et al. 2000; Peacock et al. 2000; Blain et al. 2002; Scott et al. 2002; Webb et al. 2003; van Kampen et al. 2005; Tacconi et al. 2008; Wang et al. 2010), typically because the data sets do not have enough photometric data points to precisely constrain the IR SED shape (*Herschel* data are already helping greatly in this regard; e.g., Chapman et al. 2010; Magnelli et al. 2010). Furthermore, some theoretical studies (Davé et al. 2010) have assumed that SMGs are the most rapidly star-forming galaxies in order to identify SMGs in cosmological simulations without performing RT. If SFR and submm flux density are not simply related this approach is problematic.

It is clear that a better understanding of the relationship between submm flux density and SFR and, more generally, what galaxy properties a submm galaxy selection selects for, is needed. In other work we have combined hydrodynamic simulations and dust RT to show that major mergers of massive, gas-rich disk galaxies can reproduce the $850 \mu\text{m}$ flux densities (N10), CO properties (Narayanan et al. 2009), number densities (Hayward et al. 2010, C. Hayward et al. 2011a, in preparation), AGN properties (C. Hayward et al. 2011b, in preparation), and intersection with the dust-obscured galaxy (DOG) population (Narayanan et al. 2010c) of SMGs. Motivated by the success of our simulations in reproducing a variety of SMG properties, we use them here to quantify how submm flux density depends on SFR, L_{bol} , dust content, and geometry. The aim of this study is to clarify for what galaxy properties a submm selection criterion selects and to provide a discriminant among the different modes of star formation that could power SMGs.

2. METHODS

We combine high-resolution GADGET-2 (Springel et al. 2001; Springel 2005) 3-D N-body/smoothed-particle hydrodynamics (SPH) simulations with the SUNRISE (Jonsson 2006; Jonsson et al. 2010) polychromatic Monte Carlo dust RT code in order to predict the submillimeter flux densities of high-redshift isolated and merging disk galaxies. The simulations presented here, part of a larger suite to be presented in C. Hayward et al. (2011a, in preparation), are described in N10, so here we will only summarize and describe differences from that work. This combination of GADGET-2 and SUNRISE has been successfully shown to reproduce the SEDs/colors of local SINGS (Kennicutt et al. 2003; Dale et al. 2007) galaxies (Jonsson et al. 2010); local ULIRGs (Younger et al. 2009a); massive, quiescent, compact $z \sim 2$ galaxies (Wuyts et al. 2009, 2010); 24 μm -selected galaxies (Narayanan et al. 2010c); K+A/post-starburst galaxies (G. Snyder et al. 2010, submitted), and XUV disks (Bush et al. 2010), among other populations. The success of our approach at modeling diverse galaxy populations—both local and high-redshift—lends credibility to its application to modeling SMGs.

2.1. Hydrodynamic simulations

GADGET-2 (Springel et al. 2001; Springel 2005) is a TreeSPH (Hernquist & Katz 1989) code that computes gravitational interactions via a hierarchical tree method (Barnes & Hut 1986) and gas dynamics via SPH (Lucy 1977; Gingold & Monaghan 1977). It conserves both energy and entropy (Springel & Hernquist 2002). The simulations include radiative heating and cooling as in Katz et al. (1996). Star formation is modeled via the volume-density dependent Kennicutt-Schmidt law (Kennicutt 1998a), $\rho_{\text{SFR}} \propto \rho_{\text{gas}}^{1.5}$, with a minimum density threshold; this index is consistent with observations of $z \sim 2$ disks (Krumholz & Thompson 2007; Narayanan et al. 2008a, 2010a). The structure of the ISM is modeled via a two-phase sub-resolution model in which cold, dense clouds are embedded in a diffuse, hot medium (Springel & Hernquist 2003). This medium is pressurized by supernova feedback, which heats the diffuse ISM and evaporates the cold clouds (Cox et al. 2006b). Metal enrichment is calculated by assuming each gas particle behaves as a closed box. Black hole particles accrete via Eddington-limited Bondi-Hoyle accretion and deposit 5% of their emitted luminosity—calculated from the accretion rate assuming 10% radiative efficiency, $L_{\text{bol}} = 0.1\dot{M}c^2$ —to the surrounding ISM as thermal energy (Springel et al. 2005; Matteo et al. 2005). We refer the reader to the references given above for the full details of the GADGET-2 code and the sub-resolution models employed.

We focus on two simulations, one isolated disk and one major merger. We embed exponential disks with baryonic mass $4 \times 10^{11} M_{\odot}$ in $9 \times 10^{12} M_{\odot}$ dark matter halos described by a Hernquist (1990) density profile. The disks are initially 60% gas and are scaled to $z \sim 3$ as described in Robertson et al. (2006a,b). The gravitational softening lengths are $200h^{-1}$ pc for the dark matter particles and $100h^{-1}$ pc for the star, gas, and black hole particles. We use 6×10^4 dark matter, 4×10^4 stellar, 4×10^4 gas, and 1 black hole particle per disk galaxy. For the major merger, we initialize two such disks on parabolic orbits with initial separation $R_{\text{init}} = 5R_{\text{vir}}/8$ and pericentric distance twice the disk scale length (Robertson et al. 2006b). The orbit we focus on is the ‘e’ orbit of Cox et al. (2006a). We have checked that the differences between quiescent and bursty star formation are insensitive to orbit as long as a strong starburst is induced (some orbits do not induce strong starbursts, but those are irrelevant for the purpose of studying the differences between bursty and quiescent star formation), and the larger suite of simulations (from C. Hayward et al. 2011a, in preparation) used to derive the fitting functions includes a variety of orbits.

2.2. Radiative transfer

Every 10 Myr we save snapshots of the GADGET-2 simulations and use the 3-D Monte Carlo dust RT code SUNRISE (Jonsson 2006; Jonsson et al. 2010) in post-processing to calculate the SEDs of the simulated galaxies. While we will summarize the key features of SUNRISE here, we encourage the reader to see Jonsson (2006) and Jonsson et al. (2010) for full details. Except where noted, we use the fiducial parameters given in Jonsson et al. (2010). SUNRISE calculates the emission from the stars and AGN in the GADGET-2 simulations

and the attenuation and re-emission from dust. STARBURST99 (Leitherer et al. 1999) SEDs are assigned to all star particles according to their ages and metallicities. Star particles present at the start of the GADGET-2 simulation are assigned ages assuming that their stellar mass was formed at a constant rate equal to the star formation rate of the initial snapshot and gas and stellar metallicities via a closed-box model, $Z = -y \ln f_g$, where f_g is the initial gas fraction and $y = 0.02$. Black hole particles are assigned the luminosity-dependent templates of Hopkins et al. (2007) by assuming that the bolometric luminosity of a black hole particle is $L_{\text{bol}} = 0.1\dot{M}c^2$, where \dot{M} is the black hole accretion rate from the GADGET-2 simulations.

To calculate the dust density, and thus optical depth along a given line of sight, SUNRISE projects the GADGET-2 gas-phase metal density onto a 3-D adaptive mesh refinement grid using the SPH smoothing kernel. We have assumed 40% of the metals are in dust (Dwek 1998; James et al. 2002). We use a maximum refinement level of 10, resulting in a minimum cell size of $55h^{-1}$ pc. By performing runs with higher levels of refinement we have checked that the observed-frame submm flux density is converged to within 10%. We use the Milky Way R=3.1 dust model of Weingartner & Draine (2001) as updated by Draine & Li (2007). Dust models with different FIR opacity will lead to different relationships between submm flux density and dust mass, but we show how to rescale for different values of the opacity in Equation A9.

Once the dust density grid is constructed and the input sources are assigned SEDs, SUNRISE performs Monte Carlo RT by randomly emitting photon packets from the source particles and randomly drawing interaction optical depths from the appropriate probability distribution. We use 10^7 photon packets total for each stage of the RT, having confirmed that this results in Monte Carlo noise of less than a few percent. The photon packets are scattered and absorbed by dust as they traverse the ISM. For each grid cell, the temperature of each dust species is calculated assuming the dust is in thermal equilibrium, and the dust re-emits the absorbed energy as a modified blackbody.

A SUNRISE feature key to this work is its treatment of dust self-absorption. In high-density regions, the dust can be opaque to its own emission, so the contribution of the dust emission to dust heating must be computed in addition to the contribution from stars and AGN. SUNRISE computes the equilibrium dust temperatures self-consistently by iteratively performing the transfer of the dust emission and the temperature calculation using a reference field technique similar to that of Juvela (2005). (The details of the SUNRISE implementation are in Jonsson et al. 2010 and Jonsson & Primack 2010.) This algorithm ensures accurate dust temperatures, and thus submm flux densities, even for the highly optically thick central starbursts.

The results of the SUNRISE calculation are spatially resolved, multi-wavelength (we use only 120 wavelengths here because of memory constraints) SEDs observed from 7 cameras distributed isotropically in solid angle, though in this paper we only utilize the integrated flux densities in the SCUBA (Holland et al. 1999) and AzTEC

(Wilson et al. 2008) bands. For the purpose of calculating observed flux densities we assume the simulated galaxies are at redshift $z = 2$.

2.2.1. Differences from Narayanan et al.

The primary difference between our simulations and those of N10 and Narayanan et al. (2010c) is the treatment of the ISM on sub-resolution scales. In order to model the effects of HII and photodissociation regions (PDRs), SUNRISE assigns star particles with ages less than 10 Myr SEDs from the HII region template library of Groves et al. (2008). The time-averaged fraction of solid angle obscured by the PDR, f_{PDR} , strongly affects the resulting attenuation and IR emission (for a detailed discussion see Groves et al. 2008). Narayanan et al. assumed $f_{\text{PDR}} = 1$ (so that the young stars are completely obscured by PDRs for 10 Myr) in order to match the observed range of 850 μm flux densities. Furthermore, they neglected the dust associated with the cold phase of the Springel & Hernquist (2003) ISM model, typically $\gtrsim 30\%$ of the total gas mass and $\gtrsim 90\%$ of the gas mass in the central regions for snapshots classified as SMGs.

Motivated by concerns over applicability of the Groves et al. (2008) models to the extreme ISM densities and pressures encountered in our simulations, we set $f_{\text{PDR}} = 0$, eliminating all significant dust obscuration from the sub-resolution PDR model. Instead, we use the total gas density in the SPH simulations (i.e., both the diffuse and cold phases) to calculate the dust density. Since the dust mass implicit in the Groves et al. (2008) PDRs is not tied to the total dust mass of the simulated galaxy, it is possible that one can have more dust mass in the sub-resolution PDRs than is available in the galaxy. It is also possible that the sum of the dust mass in the PDRs is less than the total available in the cold phase of the sub-resolution ISM. Our treatment ensures that neither scenario can occur.

Our assumed ISM structure (cold phase volume filling factor of unity) is similar to what is observed for the dense cores of local ULIRGs (Scoville et al. 1991; Downes & Solomon 1998; Sakamoto et al. 1999, 2008), and it leads to effective far-IR optical depths (inferred from modified blackbody fitting using $L_\nu \propto (1 - e^{-\tau_\nu})B_\nu(T_d)$; see below for details) consistent with what is observed for local ULIRGs and SMGs ($\tau = 1$ at rest-frame $\lambda \sim 200 \mu\text{m}$ for the simulations versus at rest-frame $\lambda \sim 230 - 270 \mu\text{m}$ for the ULIRGs of Lisenfeld et al. 2000 and SMGs of Lupu et al. 2010; but cf. Kovács et al. 2010). However, it is still important to note that the sub-resolution ISM structure is the key uncertainty in these calculations (Younger et al. 2009a). While unresolved clumpy dust can significantly affect the resulting SED (Witt & Gordon 1996; Városi & Dwek 1999), a more detailed treatment is beyond the scope of this work. The trends presented in this work should be qualitatively insensitive to the sub-resolution ISM assumption because, as explained below, the dominant drivers of the differences between the quiescent and bursty star formation cases are the contribution from stars formed pre-burst to the luminosity at the time of the burst and the rapid gas consumption during the burst, both of which do not depend on the treatment of sub-resolution clumpy dust.

3. RESULTS

Figure 1 shows the time evolution of the observed SCUBA 850 μm flux density (mJy), SFR ($M_\odot \text{yr}^{-1}$), bolometric luminosity L_{bol} (L_\odot), initial fraction of baryonic mass that is gas f_g , dust mass M_d (M_\odot), and dust temperature⁹ T_d (K) for the isolated disk galaxy (*left*) and merger (*right*), where all quantities except f_g have been normalized by dividing by their maximum values, given in the legend. When calculating the observed flux density we have assumed the simulated galaxy is at $z = 2$. The disk is somewhat unstable initially; after the disk settles, L_{bol} , SFR, and S_{850} decrease steadily with time. Over the 2 Gyr of the simulation the gas fraction decreases from 60% to 20%. As the gas is consumed, the SFR, and thus L_{bol} , both decrease, by factors of ~ 10 and ~ 5 , respectively. S_{850} decreases by $\sim 2.5\text{x}$. M_d also decreases as a result of the decrease in gas mass, but only by $\sim 40\%$ because the decrease in gas mass is partially mitigated by metal enrichment of the gas from star formation, as the metallicity doubles over the course of the simulation. While it may seem counter-intuitive that M_d decreases with time, for a simple closed-box model assuming dust traces metals and constant yield it can be shown (Edmunds & Eales 1998) that for $f_g \lesssim 0.6$ the dust mass increases at most by ~ 0.1 dex, and it decreases monotonically with f_g for $f_g \lesssim 0.4$. Furthermore, the preferential consumption of metal-enriched gas that occurs in our models should result in a lower dust mass than the simple closed-box case of Edmunds & Eales (1998), which assumes perfect mixing.

The behavior of the merger (Figure 1, right) is qualitatively different from that of the isolated disk. Initially, SFR, L_{bol} , and S_{850} are roughly equal to the sum of the isolated values for the two progenitor disks, because the disks are too gas-rich at first passage ($t \sim 0.1$ Gyr) for tidal torques to cause a strong starburst, as a significant stellar bar is required for the gas to efficiently lose angular momentum (Hopkins et al. 2009b). However, at final coalescence of the two disks (~ 0.7 Gyr) tidal torques induce a strong starburst, causing the SFR to increase by a factor of $\gtrsim 16$. The peak of the burst is very narrow and significant luminosity from previously formed stars remains, so the bolometric luminosity increases by a much smaller amount ($\sim 7\text{x}$) than the SFR. Moreover, as the gas is rapidly consumed in the starburst, M_d plummets by a factor of 3. Along with the more compact geometry, the decreased dust mass causes the SED to become hotter, with T_d increasing from ~ 50 K to ~ 65 K.¹⁰ The increase in dust temperature during the starburst is qual-

⁹ We have calculated T_d by fitting the modified blackbody $L_\nu \propto (1 - \exp[-(\nu/\nu_0)^\beta])B_\nu(T_d)$ to the rest-frame 20 - 1000 μm SED, allowing all parameters to vary. Here ν_0 is the frequency at which $\tau_\nu = 1$. We have assumed the opacity has a power-law dependence on ν in the IR, $\kappa_\nu \propto \nu^\beta$. Note we have not used the optically thin form $L_\nu \propto \nu^\beta B_\nu(T_d)$, as is almost always done, because we find that the first form, which does not assume optical thinness, provides a significantly better fit to our SEDs. This is because our simulated SMGs can be optically thick out to rest-frame $\gtrsim 100 \mu\text{m}$, which is supported by recent *Herschel* observations from Lupu et al. (2010), who found $\tau \sim 1$ at rest-frame $\lambda \sim 230 \mu\text{m}$. Our fitting procedure gives systematically higher T_d (by as much as 20 K) than when the optically thin form is used, so comparisons of our dust temperatures to other results should take this into account.

¹⁰ For the merger snapshots with $t \gtrsim 0.8 - 0.9$ Gyr the modified blackbody does not provide a good fit to the SED, so the dust temperature evolution beyond that time should not be trusted.

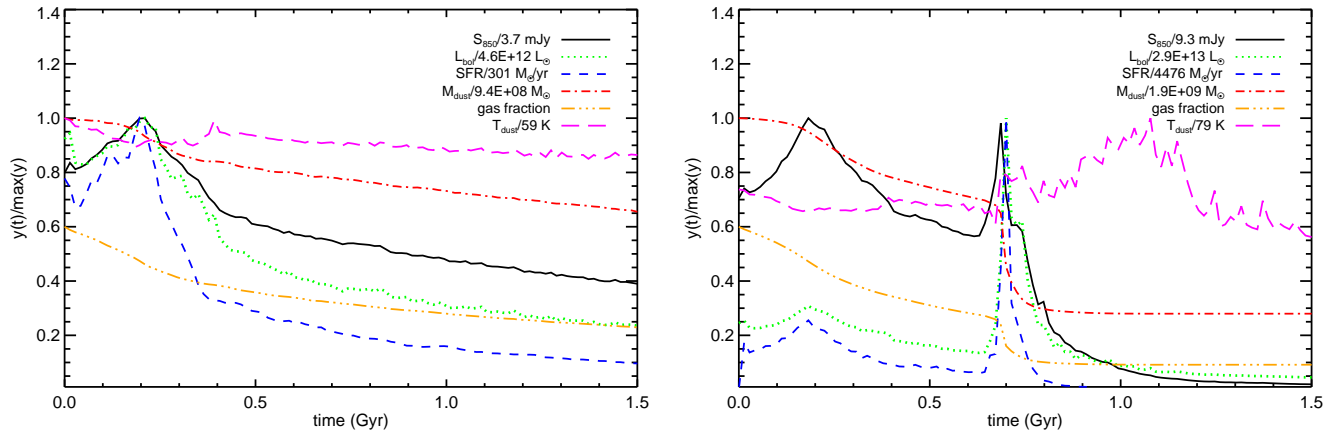


Figure 1. *Left:* The isolated disk simulation’s observed-frame integrated SCUBA 850 μm flux density (mJy, assuming $z = 2$; solid black) measured from one of the seven viewing angles, bolometric luminosity (L_{bol} ; dotted green), SFR ($M_{\odot} \text{yr}^{-1}$; dashed blue), dust mass M_d (M_{\odot} ; dash dot red), gas fraction f_g (dash dot dot orange), and dust temperature (derived from SED fitting) T_d (K; long dashed magenta) versus time (Gyr). Except for f_g , the quantities have been normalized by dividing by their maximum values, given in the legend. Once the disk reaches equilibrium, S_{850} , L_{bol} , SFR, and f_g concomitantly decrease exponentially with time as the gas is converted into stars. M_d also decreases, but by less than a factor of 2, because the decreasing f_g is offset by the increasing metallicity of the gas. T_d decreases from ~ 60 K to ~ 50 K. *Right:* Same, but for the major merger simulation. All quantities are totals for the two-disk system. Compared to the isolated disk the time evolution is more complex: Initially S_{850} , SFR, L_{bol} , and M_d are roughly just the sums of the values for the isolated progenitor disks. At first passage ($t \sim 0.1$ Gyr), the SFR is not elevated much beyond the baseline rate because the disks are very gas-rich and thus lack the massive stellar bar needed to efficiently remove angular momentum from the gas (Hopkins et al. 2009b). As the two disks coalesce ($t \sim 0.7$ Gyr), tidal torques cause a burst of star formation, resulting in the sharp increase in the SFR ($\gtrsim 16x$), L_{bol} ($\sim 7x$), and S_{850} ($\lesssim 2x$) at ~ 0.7 Gyr. The increase in L_{bol} is much less than that boost in SFR because the luminosity of the stars formed during the burst is only $\sim 6x$ the luminosity from stars already formed pre-burst. T_d increases sharply from ~ 50 K to ~ 65 K because of the strong increase in L_{bol} , concurrent decrease in M_d , and more compact geometry. This mitigates the increase in S_{850} that occurs from increased L_{bol} . The second, minor peak in L_{bol} , which occurs ~ 40 Myr after the peak SFR, corresponds to the peak AGN luminosity. Pre-coalescence, f_g decreases at a rate similar to the isolated disk case. At coalescence the gas is rapidly consumed in the central starburst. M_d decreases by a factor of 4.5, with the bulk of the decrease occurring at coalescence.

itatively consistent with observations, as local ULIRGs (i.e., merger-induced starbursts) tend to have hotter dust temperatures (~ 42 K) than less luminous (quiescent) galaxies (~ 35 K) (Clements et al. 2010). The increased T_d partially offsets the increase in S_{850} caused by the increased luminosity. The combination of the significant pre-burst contribution to L_{bol} , the small mass of stars formed in the burst, and the increased T_d cause S_{850} to increase by $\lesssim 2x$ even though the SFR increases by $\gtrsim 16x$ in the burst.

3.1. The relationship between submm flux density and SFR

Figure 2 shows the observed SCUBA 850 μm flux density in mJy versus star formation rate in units of $M_{\odot} \text{yr}^{-1}$ for the isolated disk (*left*) and major merger (*right*) viewed from all of the 7 cameras. The submm flux density of the isolated disk is tightly correlated with SFR, increasing monotonically as $\text{SFR}^{0.4}$ (see best-fit curve). This correlation occurs because once the disk settles, L_{bol} and SFR both decrease exponentially with time. The dust mass also decreases, but by less than a factor of 2 over the 2 Gyr of the simulation (see Figure 1). Both the decreased luminosity and the decreased dust mass cause the submm flux density to decrease.

The case for the major merger is again qualitatively different. Pre-coalescence, the relationships are essentially the same as for the isolated disks. This is because S_{850} , SFR, L_{bol} , and M_d at this stage are essentially just the sum of the two disks’ isolated values, and multiplying all quantities by the same factor (2 for the major merger here) does not change the power-law index. The normal-

ization of the relation is ~ 1.5 greater for the merging disks than for the isolated disk. The reason is as follows: An isolated disk of SFR s has $S_{850} = As^{0.4}$, where A is the normalization of the SFR- S_{850} relation for the isolated disk. For a non-interacting system of two identical disks to have total SFR equal to that of the single isolated disk, the two disks must each have $\text{SFR} = 0.5s$. Thus the total submm flux density of the system is the submm flux density of a single disk of SFR $0.5s$, which we calculate using the isolated relation, multiplied by 2. This is $S_{850} = 2A(0.5s)^{0.4} = 1.5As^{0.4}$. Therefore the normalization of the SFR- S_{850} relation for the sum of two identical disks is 1.5 times that of the individual disk relation. This fact has important implications for the SMG population, which we discuss in §4.2.

On the other hand, the merger-induced burst is significantly less effective at boosting the submm flux density. For a given SFR, the submm flux density is significantly less than for the isolated and pre-coalescence (quiescent star formation) cases. This is because of two reasons: 1. The sharp decrease in dust mass and more compact geometry cause an increase in dust temperature, mitigating the increase in S_{850} caused by increased L_{bol} . 2. The significant luminosity contributed by stars formed before the starburst causes L_{bol} to increase sub-linearly with SFR. During the burst, $L_{\text{bol}} \approx L_{\text{pre-peak}} + \alpha \text{SFR}$, where α is the luminosity per unit star formation rate for an instantaneous burst. Thus L_{bol} is not proportional to SFR when $L_{\text{pre-peak}}$ is non-negligible compared to the luminosity of newly-formed stars, which is the case here because a relatively small fraction of the stellar mass is formed in the sharp, short-duration burst. For the burst,

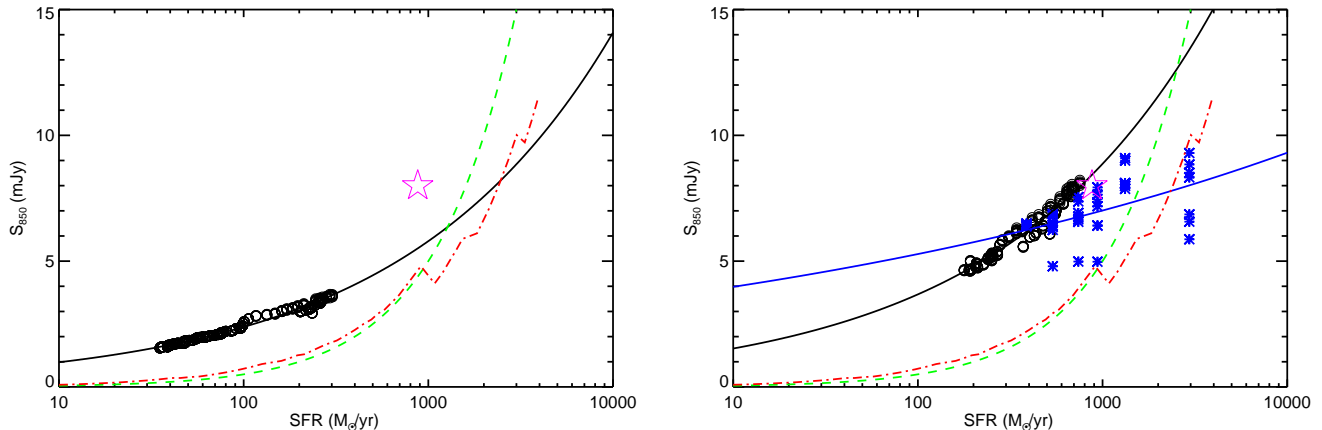


Figure 2. Integrated SCUBA 850 μm flux density (mJy) versus SFR ($M_{\odot} \text{yr}^{-1}$) for the isolated disk (*left*) and major merger (*right*) viewed from all of the 7 different cameras. The best-fit power laws (solid lines), linear relation $S_{850} = 0.5 \text{ mJy} (\text{SFR}/100 M_{\odot} \text{yr}^{-1})$ (green dashed lines; obtained using the $S_{850} - L_{\text{IR}}$ relation from Neri et al. 2003 and Equation A11), the relation for the Chary & Elbaz (2001) templates (red dash dot), and the value for the Pope et al. (2008) composite SED (magenta star) are also shown. (The last two were obtained by redshifting the templates to $z = 2$ and converting L_{IR} of each template to SFR using Equation A11.) For the isolated disk, the submm flux density is tightly correlated with both SFR and L_{bol} , increasing essentially monotonically as $\text{SFR}^{0.4}$. For the major merger, pre-coalescence (black open circles) the power-law index is the same as for the isolated disks because the SFR, L_{bol} , dust mass, and submm flux density are essentially two times the isolated disk values (see Figure 1), so only the normalization changes. During the coalescence-induced starburst (blue asterisks), the relationship is significantly shallower, with submm flux density scaling as $\text{SFR}^{0.1}$. This is due to two effects: 1. The stars formed before the peak of the starburst contribute significantly to L_{bol} at the starburst peak, so $L_{\text{bol}} \not\propto \text{SFR}$. 2. The rapid gas consumption during the burst causes M_d to plummet, and the decrease in dust mass and more compact geometry cause T_d to increase sharply, mitigating the increase of S_{850} caused by the increased L_{bol} . Note that $S_{850} \propto \text{SFR}$ (green dashed line) is a poor assumption, as are the Chary & Elbaz (2001) templates. However, we do not necessarily expect the latter to work in this case, because at high redshift ULIRG SEDs are often better fit by local templates appropriate for less luminous (colder) galaxies (e.g., Pope et al. 2006; Dannerbauer et al. 2010; Rex et al. 2010). The Pope et al. (2008) template agrees well because it accounts for the colder nature of high- z galaxies, but since it is a single composite SED it does not provide a relationship between SFR and S_{850} to which we can compare.

the submm flux density scales as $\text{SFR}^{0.1}$ (see best-fit curve), significantly more weakly than for quiescent star formation, and the ratio of submm flux density to SFR is significantly lower. Hence, bursts of star formation are significantly less effective at boosting submm flux density than one might naively expect.

It is interesting to note that, during the starburst, the observed submm flux density can vary significantly with viewing angle (e.g., for the snapshot with peak SFR, S_{850} varies in the range $\sim 6 - 9$ mJy depending on the camera). We have confirmed that this variation is due to dust self-absorption: the central regions of the starburst can be so obscured that even the IR emission is significantly anisotropic. As a result, the dust temperature, and thus submm flux density, depends on the line of sight. Though we will not explore this possibility further in this work, we note that differences in viewing angle may be enough to account for the spread of dust temperatures observed for high- z ULIRGs. In other words, from one viewing angle a simulated galaxy may be identified as an SMG whereas from another viewing angle the same galaxy could be identified as a hot-dust-dominated ULIRG undetected in the submm.

3.2. Dependence of submm flux density on SFR, L_{bol} , and M_d

For a given SFR, galaxies of different masses tend to also have different dust masses; thus the normalization of the S_{850} -SFR relation varies for different mass simulations though the scalings are similar. As a result, one cannot calculate the submm flux density given only the SFR, but it is possible to parameterize the submm flux

density as a function of SFR and dust mass. Since much of the discrepancy in the S_{850} -SFR relations for quiescent and bursty star formation is caused by the rapid decrease in dust mass during the starburst, we expect that including dust mass in our parameterization will eliminate much of the difference between quiescent and bursty star formation modes. We have analyzed the full set of simulations from our SMG number counts work (Hayward et al. 2010, C. Hayward et al. 2011a, in preparation), which includes a range of progenitor disk baryonic masses ($\sim 3.5 \times 10^{10} - 4 \times 10^{11} M_{\odot}$), mass ratios ($\sim 0.1 - 1$), and initial gas fractions ($0.6 - 0.8$), fitting the submm flux density as a power law in both SFR and dust mass. Perhaps surprisingly, the following relations (for simulated galaxies placed at redshift $z = 2$) hold to within ~ 0.1 dex for all but a few outliers over the range $0.5 \text{ mJy} \lesssim S_{850} \lesssim 15 \text{ mJy}$:

$$S_{850} = 0.65 \text{ mJy} \left(\frac{\text{SFR}}{100 M_{\odot} \text{yr}^{-1}} \right)^{0.42} \left(\frac{M_d}{10^8 M_{\odot}} \right)^{0.58} \quad (1)$$

$$S_{1.1} = 0.30 \text{ mJy} \left(\frac{\text{SFR}}{100 M_{\odot} \text{yr}^{-1}} \right)^{0.36} \left(\frac{M_d}{10^8 M_{\odot}} \right)^{0.61}$$

We can also fit the submm flux density as a function of L_{bol} and M_d :

$$S_{850} = 0.40 \text{ mJy} \left(\frac{L_{\text{bol}}}{10^{12} L_{\odot}} \right)^{0.52} \left(\frac{M_d}{10^8 M_{\odot}} \right)^{0.60} \quad (2)$$

$$S_{1.1} = 0.20 \text{ mJy} \left(\frac{L_{\text{bol}}}{10^{12} L_{\odot}} \right)^{0.46} \left(\frac{M_d}{10^8 M_{\odot}} \right)^{0.63}$$

These fitting functions are accurate to within ~ 0.15 dex.

Replacing L_{bol} with L_{IR} , the IR luminosity inferred by an observer, yields a similar result. Figure 3 shows how well these fitting functions reproduce the submm flux density of our simulated galaxies. It is discussed in more detail in §3.2.2.

3.2.1. Relations for an optically thin modified blackbody

It is instructive to compare the above relations to those for a single-temperature mass of dust transparent to its own emission, the model which is implicit in the standard method of fitting a modified blackbody to the IR SED. For a mass of dust in thermal equilibrium with temperature T_d we can express the submm flux density as a function of dust bolometric luminosity L_d and dust mass M_d or SFR and M_d . Assuming $z = 2$ and far-IR spectral index $\beta = 2$, the relations are (see the Appendix for a derivation)

$$S_{850} = 1.4 \text{ mJy} \left(\frac{\text{SFR}}{100 M_{\odot} \text{ yr}^{-1}} \right)^{1/6} \left(\frac{M_d}{10^8 M_{\odot}} \right)^{5/6} \quad (3)$$

and

$$S_{850} = 1.4 \text{ mJy} \left(\frac{L_d}{10^{12} L_{\odot}} \right)^{1/6} \left(\frac{M_d}{10^8 M_{\odot}} \right)^{5/6}. \quad (4)$$

These should be compared to Equations (1) and (2), respectively, by assuming $L_{\text{bol}} \approx L_d$ (i.e., the luminosity emitted by stars and AGN is completely absorbed by dust), which is a reasonable approximation for snapshots classified as SMGs ($S_{850} > 3$ mJy).

3.2.2. Comparison of the relations to the full radiative transfer

Figure 3 shows the logarithm of the ratio of the submm flux density calculated using the above equations ($S_{850, \text{analytic}}$) to the submm flux density calculated through the RT ($S_{850, \text{RT}}$) versus $S_{850, \text{RT}}$. The left panel shows the results when Equations (1, black circles) and (3, blue triangles) are used to calculate S_{850} from SFR and M_d . The right panel shows the results when L_{bol} and M_d are used instead, with the black circles corresponding to Equation (2) and the blue triangles Equation (4). The fitting functions derived from the simulations are able to reproduce S_{850} from SFR (L_{bol}) and M_d to within ~ 0.1 (0.15) dex. The simple modified blackbody model tends to overpredict the submm flux density by $\gtrsim 0.3$ dex; the typical over-prediction is ~ 0.5 dex (a factor of 3). (Note that the corresponding uncertainties in SFR, L_{bol} , and M_d for fixed observed submm flux density would be less because the submm flux density scales with these quantities sublinearly.) Furthermore, the error in the prediction correlates with SFR (L_{bol}) and dust mass because of the differences in the power-law indices for the fitting functions and the modified blackbody relations.

The optically thin modified blackbody model fails for multiple reasons. From SED fitting we find that the simulated galaxies can have effective optical depth $\tau > 1$ out to rest-frame $\sim 200 \mu\text{m}$. For fixed dust temperature, the optically thin assumption will result in an overestimate of the luminosity density at wavelengths for which $\tau \gtrsim 1$ because $(1 - \exp[-(\nu/\nu_0)^\beta]) < (\nu/\nu_0)^\beta$ for all $\nu > 0$. Thus Equation (A3) will overestimate L_d for fixed T_d and M_d .

If L_d and M_d are fixed, the dust temperature will be *underestimated* when optical thinness is assumed, and, therefore, the submm flux density will be overestimated. Also, $L_d \approx L_{\text{bol}}$ is less accurate an approximation for the faintest sources than for the brightest because L_d/L_{bol} increases with L_{bol} (Jonsson et al. 2006). If $L_d < L_{\text{bol}}$, the assumption that $L_d \approx L_{\text{bol}}$ will overestimate L_d and thus overestimate the submm flux density; this may explain why the overprediction is worse for lower S_{850} . Finally, we have seen above that the assumption $L_{\text{bol}} \propto \text{SFR}$ is invalid during the burst.

4. DISCUSSION

We have demonstrated that the submm flux density of a galaxy scales differently with SFR for quiescent and bursty star formation. The ratio of sub-mm flux density to SFR is significantly less for merger-induced bursts than for quiescent star formation. This is because of the rapid decrease in dust mass and more compact geometry during the starburst, which causes the SED to become hotter, and the significant contribution from stars formed pre-burst to the luminosity during the burst, which makes the luminosity increase by a much smaller factor than the SFR. As a result, merger-induced starbursts are less efficient at boosting submm flux density than one might naively expect.

Our results have a number of important implications; we discuss these now.

4.1. Predicting submm flux densities from models

One implication of this study is that the galaxies with highest submm flux density are not necessarily those with the highest bolometric luminosities or SFRs. Thus theoretical models, be they simulations or semi-analytic, must explicitly calculate the submm flux density of their simulated galaxies in order to select which are SMGs as opposed to simply selecting the most rapidly star-forming or most luminous objects. However, the computational expense required to self-consistently calculate the submm flux density limits this approach to idealized, non-cosmological simulations (as done here), individual galaxies excised from cosmological zoom-in simulations, or semi-analytic models in which various simplifying assumptions must be made. As an alternative to performing RT, cosmological simulations and semi-analytic models can use the relations among submm flux density, SFR or bolometric luminosity, and dust mass presented herein (Equations 1 and 2) to assign submm flux density to simulated galaxies. Additionally, observers can use the relations to estimate the instantaneous SFR given submm flux density and dust mass (obtained from fitting the IR SED using the full modified blackbody as we have done or by measuring the gas mass and assuming a dust-to-gas ratio; ignoring uncertainties on submm flux density, a dust mass accurate to a factor of 2 gives SFR accurate to a factor of 3).

4.2. Heterogeneity of the SMG population

These results also imply that the SMG population is heterogeneous. We have seen that it is possible for a quiescently star-forming disk to have submm flux density equal to that of a merger with much higher SFR (Figure 2). Furthermore, since the scaling of submm flux density

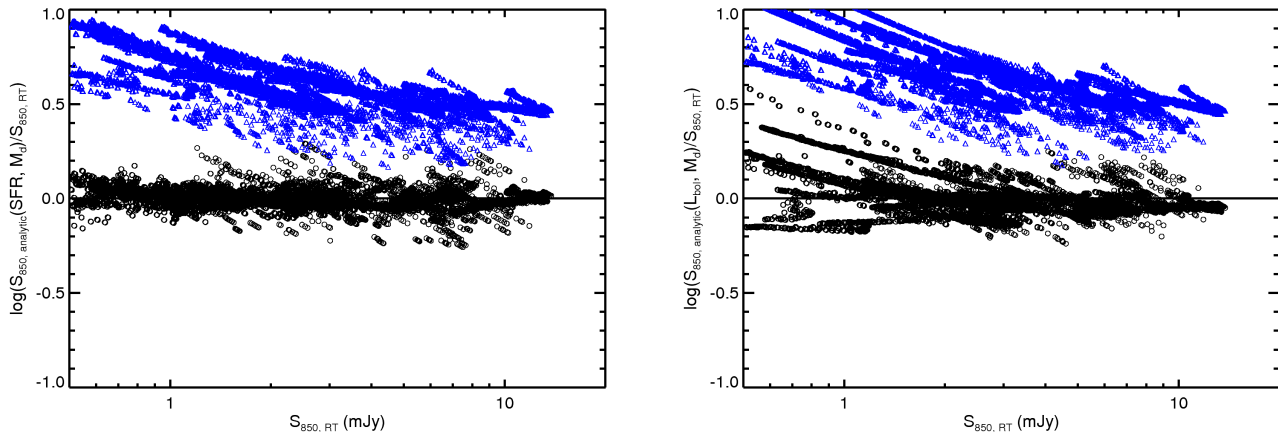


Figure 3. *Left:* Logarithm of the ratio of the submm flux density calculated using one of the analytic forms ($S_{850,\text{analytic}}$) to the submm flux density calculated through the full RT ($S_{850,\text{RT}}$) vs. $S_{850,\text{RT}}$ for all time snapshots of our simulated galaxies. Black circles show the ratio when $S_{850,\text{analytic}}$ is calculated from the SFR and M_d of our simulated galaxies using Equation (1). Blue triangles show the ratio when the optically thin modified blackbody model (Equation 3) is used. The line $S_{850,\text{analytic}} = S_{850,\text{RT}}$ is shown to guide the eye. *Right:* Same, except now the black circles show the values when Equation (2) is used to calculate the submm flux density from L_{bol} and M_d of the simulation snapshots, and the blue triangles show the values when Equation (4) is used, assuming $L_{\text{bol}} \approx L_d$. In both cases the simple optically thin modified blackbody model overpredicts the submm flux density by $\gtrsim 0.3$ dex for the simulated SMGs, and the overprediction is worse for lower S_{850} .

with SFR is sublinear, adding two equal disks (and thus doubling the dust mass and SFR of the system) increases the submm flux density more than simply boosting the SFR by a factor of 2; Equation (1) shows that SFR would have to be boosted by 5x to achieve a 2x boost in submm flux density if dust mass is kept constant. When the sharp increase in dust temperature during the starburst and the narrowness of the burst are accounted for the effect becomes even stronger: in Figure 1 we see that a $\gtrsim 16x$ increase in SFR gives a $\lesssim 2x$ increase in submm flux density.

The submm bolometers used for wide-field surveys of SMGs have beam sizes $\gtrsim 15''$ ($\gtrsim 130$ kpc at $z = 2$). Thus, during a merger the two progenitor galaxies will spend a considerable amount of time within the area of the beam. From the above arguments, we see that this is a very efficient way to create an SMG, but this contribution has been relatively unappreciated. We argue that the SMG population attributable to mergers is bimodal: some are merger-induced starbursts and some are two (or more) infalling disks (normal galaxies that are not yet interacting strongly) blended into one submm source (“galaxy pair SMGs”).¹¹ Note also that not only major mergers but also favorably oriented minor mergers (see, e.g., Cox et al. 2008; Hopkins et al. 2009b) can contribute to the SMG population.

Furthermore, the most massive, rarest ‘isolated disks’,

¹¹ Wang et al. (2010) recently presented high-resolution submm continuum images of two SMGs which were previously identified as single sources but are resolved as 2 or 3 distinct submm sources in their images. The sources are at significantly different redshifts and thus physically unrelated. Our galaxy pair SMGs are also two sources blended into one, but they are distinct from the type of SMGs Wang et al. observed because they are physically connected because they are merging. Both types of blended sources are potentially important SMG subpopulations that complicate our understanding of SMGs, and it is crucial to understand the relative contributions of merger-induced starbursts, galaxy pair/infall-stage mergers, quiescently star-forming disks, and physically unrelated, blended sources.

and even small groups, may also contribute; we expect this contribution to be subdominant because SMGs are on the exponential tail of the mass function, but we defer a precise determination of their contribution to future work. Though both the merger-induced starburst and galaxy pair populations are mergers, only in the former is the star formation merger-driven (and only partially, as the baseline star formation that would occur in the disks even if they were not interacting is significant). Given that the physically meaningful property of local ULIRGs is not that their IR luminosities are $\geq 10^{12} L_{\odot}$ but that they are powered by merger-driven star formation and AGN, only the merger-driven starburst category of SMGs should be considered physically analogous to local ULIRGs.

The observational signatures and physical implications of this bimodality will be discussed in future work. Here we simply note that the galaxy pair contribution is supported observationally by the frequency of multiple radio (Ivison et al. 2002, 2007; Younger et al. 2009c), 24 μm (Pope et al. 2006), and 350 μm (Kovács et al. 2010) counterparts to SMGs; by CO interferometry showing that a large fraction of SMGs are resolved binaries (Tacconi et al. 2006, 2008; Bothwell et al. 2010; Engel et al. 2010); and by the SMGs that have morphologies that do not resemble merger remnants (e.g., Bothwell et al. 2010; Carilli et al. 2010).¹²

4.3. SMG masses

The masses of SMGs are hotly debated, with different authors finding masses discrepant by $\sim 6x$ for the same SMGs (Michałowski et al. 2010a,b; Hainline et al. 2010). Accurate masses are important in order to test potential evolutionary relationships among

¹² Note, however, that the Bothwell et al. (2010) and Carilli et al. (2010) objects that resemble disk galaxies may in fact be the molecular disks that re-form rapidly after a gas-rich merger (Narayanan et al. 2008b).

SMGs and other galaxy classes (e.g., Brodwin et al. 2008; Bussmann et al. 2009a,b; Narayanan et al. 2010c; Rothberg & Fischer 2010) and to check that number densities of SMGs are consistent with observed stellar mass functions. Stellar mass determinations from SED fitting are limited by uncertainties in stellar evolution tracks, the initial mass function, star formation histories, dust attenuation, and AGN contamination. Since our models use star formation histories, attenuation (from the geometry of stars, AGN, and dust), and AGN components that originate directly from the hydrodynamic simulations instead of the standard assumptions—e.g., instantaneous burst or exponential star formation histories, the Calzetti attenuation law (Calzetti et al. 1994, 2000; Calzetti 1997)—we can provide constraints on SMG stellar masses that are complementary to those derived from SED fitting.

Given the inefficiency of bursts at boosting submm flux density that we have demonstrated above, SMGs must be very massive, because smaller galaxies undergoing even very strong bursts cannot make SMGs. Our models require $M_\star \gtrsim 6 \times 10^{10} M_\odot$ to reach $S_{850} \gtrsim 3$ mJy, and typical masses are higher. The area of the $S_{850} - M_\star$ plot spanned by our models agrees well with the observationally derived values of Michałowski et al. (2010a). About half of the Hainline et al. (2010) values lie in the area spanned by our models, whereas the other half have lower masses. However, the single-component star formation histories assumed by Hainline et al. may cause the stellar masses to be underestimated by $\sim 2x$, which would resolve much of the discrepancy. A detailed comparison of the mass estimates will be presented in M. Michałowski et al. (2011, submitted).

4.4. SMG duty cycles

Understanding the duty cycle of SMGs is important for predicting submm counts from models, quantifying the contribution of SMGs to stellar mass buildup, and interpreting star formation efficiencies of SMGs. Since the submm flux density depends on luminosity heating the dust, dust mass, and geometry, the submm duty cycle depends on the same factors. As we have seen, the starburst induced at merger coalescence causes a sharp peak in SFR, L_{bol} , and submm flux density. However, the duty cycle is limited because of the sharp cutoff in SFR, and thus drop in L_{bol} , after the burst and the significant drop in dust mass that occurs as highly enriched gas is consumed in the burst.

Since the submm flux density depends more strongly on dust mass than either SFR or L_{bol} (see Equations 1 and 2), it is more efficient if one can keep more dust around at the expense of lower star formation rate. The quiescent star formation mode does exactly this. As a result, the galaxy pair phase (discussed in §4.2) adds significantly to the submm duty cycle. Figure 1 shows that the galaxy pair phase has a longer submm duty cycle than the burst, though the lack of smooth accretion in our simulations—and thus need for starting with very high initial gas fractions—complicates a precise determination of the relative flux densities and duty cycles of the galaxy pair and starburst phases. Regardless, it is clear that the galaxy pair phase increases the SMG duty cycle significantly, alleviating some of the tension between the submm counts estimated from high-redshift major

merger rates and short (~ 100 Myr) starburst duty cycles by Davé et al. (2010) and the observed submm counts. Inclusion of both SMG populations is crucial to match the observed SMG number counts without resorting to a top-heavy initial mass function (Hayward et al. 2010, C. Hayward et al. 2011a, in preparation).

4.5. Implications for IR SED fitting

One reason the single temperature, optically thin modified blackbody fails is that the effective optical depth of our simulated SMGs can be greater than 1 out to rest-frame $\sim 200 \mu\text{m}$. This is consistent with the effective optical depths derived by Lupu et al. (2010) when they fit a general modified blackbody (i.e., not assuming optical thinness) to the IR SEDs of their SMGs. By assuming optical thinness and only fitting longward of the FIR peak, one overestimates the luminosity density at wavelengths for which $\tau \gtrsim 1$ (see §3.2.2).¹³ Consequently, the assumption of optical thinness yields a colder dust temperature (by as much as ~ 20 K) than if optical thinness is assumed.

In the pre-*Herschel* era, often flux densities in only a few FIR bands and at 1.4 GHz were available for large samples of SMGs. As a result of the limited number of data points, models more complex than the optically thin modified blackbody (e.g., the full modified blackbody used here or models assuming a distribution of temperatures) could not provide a better description of the data (e.g., Kovács et al. 2006). However, now that *Herschel* PACS (Magnelli et al. 2010) and SPIRE (Chapman et al. 2010) have provided data over the entire FIR SED for large samples of SMGs it is possible to perform more sophisticated fitting. Given the physical inferences that are drawn from effective dust temperatures obtained via FIR SED fitting, it is important to have as robust a method as possible and to take full advantage of the available data. We will present such a method in future work.

4.6. Limitations of our model

At this point we find it instructive to define the limitations of this work so that the results can be placed in an appropriate context and future experiments can be designed for maximal impact. One of the primary limitations, both for the radiative transfer and the hydrodynamics, is the treatment of the sub-resolution interstellar medium, especially—because we focus upon the submm flux—the structure, distribution, and composition of the dust which dominates emission at submm wavelengths. In fact, the differences between the model employed in this work and that we used in N10 were motivated by a desire for a simpler treatment of the sub-resolution ISM (see §2.2.1). In N10, stars with age ≤ 10 Myr dominated the submm flux, so the submm flux was closely tied to the SFR (see Fig. 1 of N10). Our simplified assumptions (no sub-resolution PDR model, uniform ISM density on scales below the SPH smoothing length) result in submm flux that is tied more directly to the bolometric luminosity than the instantaneous star formation rate because

¹³ This may explain why Pope et al. (2006) found that the submm flux density tends to overpredict L_{IR} , and the overprediction is worse for SMGs at low redshift where the SED is sampled further from the IR peak.

stars with age > 10 Myr contribute significantly to the bolometric luminosity and, because they are still deeply embedded in dust, the submm flux.

While our model has the advantages of simplicity and strict physical consistency (because the obscuration originates purely from the hydrodynamic simulations rather than from sub-resolution PDRs), we still must make an assumption about the sub-resolution structure of the ISM. By assuming uniform density on scales below the smoothing length we only include clumpiness that arises from the hydrodynamic simulations, so this assumption may be considered conservative. The assumption is also simplistic, of course, because the real ISM has significant structure on scales $\lesssim 100$ pc. However, proper treatment of radiative transfer through a clumpy medium is a significant area of research in and of itself (e.g., Hobson & Padman 1993; Witt & Gordon 1996; Városi & Dwek 1999) and thus beyond the scope of this work. A study of the effects of sub-resolution dust clumpiness on galaxy SEDs and efforts to devise a better treatment of sub-resolution dust clumpiness in SUNRISE are underway.

We also caution that the ISM treatment in the hydrodynamical simulations themselves can affect both the amplitude and duration of bursts of star formation (Cox et al. 2006b; Springel et al. 2005). However, while the ISM treatment may change the relative contribution of quiescent and bursty star formation to the star formation history of a given merger, it should not change the differences between quiescent and bursty star formation which lead to the significantly different relationships between SFR and submm flux, so this uncertainty has a relatively limited influence on our results. Ongoing and future studies, with much higher resolution and more advanced tracking of the clumpy ISM, will improve the predictive power of our models.

Furthermore, we stress that the simulations presented here are not cosmological. We adopt this approach because it enables us to achieve the high resolution necessary to perform radiative transfer in order to accurately calculate the submm flux density; to survey the parameter space of progenitor masses, mass ratios, and orbits; and to avoid uncertainties in modeling realistic galaxy populations in a cosmological environment. The primary drawback of this approach for our present purposes is the lack of gas accretion, which cosmological hydrodynamic simulations show is a significant driver of star formation for the high-redshift, massive galaxies with which we are concerned (Kereš et al. 2005, 2009). Gas accretion can continually replenish the gas in the galaxy, maintaining relatively high gas fractions and relatively constant star formation histories (e.g., Davé et al. 2010).

Inclusion of cosmological gas accretion would alter the time evolution presented in Figures 1, but it would not significantly alter the differences between the quiescent and merger-induced burst modes of star formation. This is because mergers would still superimpose a strong burst of star formation and sharp decrease in gas mass over the baseline evolution. Furthermore, unless smooth accretion significantly affects the geometry of stars and dust in the simulated galaxies, it will not have a significant effect on the relationship between submm flux, L_{bol} , and dust mass (the relationship between submm flux, SFR, and dust mass may be more affected because the relation

between SFR and L_{bol} may be changed significantly). Thus inclusion of cosmological gas accretion should not qualitatively alter our results.

4.7. Connections to previous work

In previous work, we developed a model relating the evolution of galaxies, starbursts, and quasars (Hopkins et al. 2006a,b, 2008a, 2009d; Somerville et al. 2008). A principal conclusion from these analyses is that while starbursts driven by gas-rich mergers can account for many instances of unusual activity in galaxies, they provide only a minor contribution to the star formation history of the Universe (Hopkins et al. 2006c). Indeed, Hopkins et al. (2010) emphasize that much of the star formation during galaxy interactions occurs in the “quiescent” mode and should not be counted as part of a merger-induced starburst. This is supported by the decomposition of the light profiles of nearby ongoing mergers (Hopkins et al. 2008b) and local cusp (Hopkins et al. 2009a) and core (Hopkins et al. 2009c) ellipticals. All of these objects exhibit evidence of “excess” central light (Rothberg & Joseph 2004; Kormendy et al. 2009), indicative of relic starbursts (Mihos & Hernquist 1994, 1996) caused by merger-driven inflows of gas (Barnes & Hernquist 1991, 1996). The integrated mass in these components agrees well with estimates of the cosmic history of merger-induced starbursts (Hopkins & Hernquist 2010).

The results presented herein extend these conclusions to high-redshift phenomena. Critically, we find that “quiescent” star formation during galaxy interactions, i.e., star formation which occurs during the infall/pair stage, is a key element in understanding the brightest submm sources, especially their number counts and duty cycles, and connecting them to other high-redshift populations including quasars (Hopkins et al. 2008a; Narayanan et al. 2008b) and compact spheroidal galaxies (Wuyts et al. 2009, 2010). Just as nearby LIRGs represent a heterogeneous collection of merging and isolated systems, it is natural to suggest that the population of high-redshift submm galaxies is heterogeneous, as we have argued here.

5. CONCLUSIONS

We have combined high-resolution 3-D hydrodynamic simulations of high-redshift isolated and merging disk galaxies and 3-D Monte Carlo dust radiative transfer calculations to study the submillimeter galaxy selection, focusing on the relationships among submm flux density, star formation rate, bolometric luminosity, and dust mass. Our main conclusions are the following:

1. The relationship between SFR and submm flux density differs significantly for quiescent and bursty star formation modes. Starbursts produce significantly less submm flux density for a given SFR, and the scaling between submm flux density and SFR is significantly weaker for bursts than for quiescent star formation. Bursts are a very inefficient way to boost submm flux density (e.g., a starburst that increases SFR by $\gtrsim 16x$ increases submm flux density by $\lesssim 2x$). Another consequence is that the galaxies with highest submm flux density are not

- necessarily those with highest SFR or bolometric or infrared luminosity.
2. The submm flux density of our simulations can be parameterized as a power law in SFR and dust mass (L_{bol} and dust mass) to within $\sim 0.1(0.15)$ dex. The scaling derived from the commonly used optically thin modified blackbody model systematically overpredicts the submm flux density by $\gtrsim 2x$ because numerous assumptions of the model (optical thinness in the FIR, $L_{\text{IR}} \propto \text{SFR}$, $L_{\text{bol}} \approx L_{\text{IR}}$) do not hold. The fitting functions we provide (Equations 1 and 2) should be useful for calculating the flux density in semi-analytical models and cosmological simulations when full radiative transfer cannot be performed and for interpreting observations.
 3. Mergers create SMGs through another mechanism besides the strong starburst induced at coalescence—they cause the two infalling disks to be observed as one submm source because both disks will be within the large ($\sim 15''$, or 130 kpc at $z = 2$) beam of the submm bolometers used to identify SMGs during much of the infall stage. For major mergers, this effect boosts the submm flux density by $2x$. To achieve the same boost in submm flux density one would have to boost the SFR of a quiescent disk by $\sim 6x$ or induce a starburst that boosts the SFR by $\gtrsim 16x$. This implies that the SMG population is heterogeneous: it is composed of both late-stage major mergers and two (or more) infalling disks observed as a single submm source (“galaxy pair SMGs”). The largest quiescent star-forming galaxies may also contribute. Thus, unlike local ULIRGs, SMGs are a mix of quiescent and bursting sources.
 4. SMGs must be very massive: to reach $S_{850} \gtrsim 3$ mJy, stellar mass of at least $6 \times 10^{10} M_{\odot}$ is required, and typical values are higher.
 5. The submm duty cycles of our simulated galaxies are a factor of a few longer than what one would expect if all SMGs were merger-driven bursts because the relatively gentle decline in SFR, L_{bol} , and dust mass during the galaxy pair phase results in a longer duty cycle for the galaxy pair phase than for the starburst. The duty cycle of the latter is limited because the peak in luminosity is narrow and the dust temperature increases sharply during the burst.
 6. Fitting the SEDs of SMGs with an optically thin modified blackbody tends to yield significantly lower dust temperatures than when the full opacity term is used because the effective optical depths can be ~ 1 out to rest-frame $\sim 200 \mu\text{m}$, both for our simulated SMGs and observed SMGs. Therefore, one should be cautious when interpreting effective dust temperatures derived via fitting an optically thin modified blackbody to the FIR SED, especially when comparing SMGs to galaxies for which optical thinness in the IR may be a reasonable approximation.

Future work will include predictions of submm number counts from our model, an investigation of the observational signatures and physical implications of the proposed SMG bimodality, a study of the AGN contribution to our model SMGs, and an improved method for fitting IR SEDs of galaxies.

CCH thanks Scott Chapman, Emanuele Daddi, Phil Hopkins, Brandon Kelly, Chris McKee, Diego Munoz, Alex Pope, Barry Rothberg, Greg Snyder, and Josh Younger for useful discussion and Jeff Pettibone for hospitality which facilitated the writing of this paper. We thank Volker Springel for providing the non-public version of GADGET-2 used for this work. DK is supported by NASA through Hubble Fellowship grant HST-HF-51276.01-A. PJ acknowledges support by a grant from the W. M. Keck Foundation. The simulations in this paper were performed on the Odyssey cluster supported by the FAS Research Computing Group at Harvard University.

REFERENCES

- Alexander, D. M., Bauer, F. E., Chapman, S. C., Smail, I., Blain, A. W., Brandt, W. N., & Ivison, R. J. 2005a, *ApJ*, 632, 736
 Alexander, D. M., Smail, I., Bauer, F. E., Chapman, S. C., Blain, A. W., Brandt, W. N., & Ivison, R. J. 2005b, *Nature*, 434, 738
 Alexander, D. M., et al. 2008, *AJ*, 135, 1968
 Barger, A. J., Cowie, L. L., Sanders, D. B., Fulton, E., Taniguchi, Y., Sato, Y., Kawara, K., & Okuda, H. 1998, *Nature*, 394, 248
 Barnes, J., & Hernquist, L. 1991, *ApJ*, 370, L65
 —. 1996, *ApJ*, 471, 115
 Barnes, J., & Hut, P. 1986, *Nature*, 324, 446
 Baugh, C. M., Lacey, C. G., Frenk, C. S., Granato, G. L., Silva, L., Bressan, A., Benson, A. J., & Cole, S. 2005, *MNRAS*, 356, 1191
 Biggs, A. D., & Ivison, R. J. 2008, *MNRAS*, 385, 893
 Blain, A. W., Smail, I., Ivison, R. J., Kneib, J.-P., & Frayer, D. T. 2002, *Phys. Rep.*, 369, 111
 Bothwell, M. S., et al. 2010, *MNRAS*, 405, 219
 Bouché, N., et al. 2007, *ApJ*, 671, 303
 Brodwin, M., et al. 2008, *ApJ*, 687, L65
 Bush, S. J., Cox, T. J., Hayward, C. C., Thilker, D., Hernquist, L., & Besla, G. 2010, *ApJ*, 713, 780
 Bussmann, R. S., et al. 2009a, *ApJ*, 693, 750
 —. 2009b, *ApJ*, 705, 184
 Calzetti, D. 1997, *AJ*, 113, 162
 Calzetti, D., Armus, L., Bohlin, R. C., Kinney, A. L., Koornneef, J., & Storchi-Bergmann, T. 2000, *ApJ*, 533, 682
 Calzetti, D., Kinney, A. L., & Storchi-Bergmann, T. 1994, *ApJ*, 429, 582
 Capak, P., et al. 2008, *ApJ*, 681, L53
 Carilli, C. L., et al. 2010, *ApJ*, 714, 1407
 Casey, C. M., Chapman, S. C., Smail, I., Alaghband-Zadeh, S., Bothwell, M. S., & Swinbank, A. M. 2010, *arXiv:1009.5709*
 Casey, C. M., et al. 2009, *MNRAS*, 399, 121
 Chakrabarti, S., Fenner, Y., Cox, T. J., Hernquist, L., & Whitney, B. A. 2008, *ApJ*, 688, 972
 Chakrabarti, S., & McKee, C. F. 2005, *ApJ*, 631, 792
 —. 2008, *ApJ*, 683, 693
 Chapman, S. C., Blain, A. W., Smail, I., & Ivison, R. J. 2005, *ApJ*, 622, 772
 Chapman, S. C., Smail, I., Blain, A. W., & Ivison, R. J. 2004, *ApJ*, 614, 671
 Chapman, S. C., Windhorst, R., Odewahn, S., Yan, H., & Conselice, C. 2003, *ApJ*, 599, 92
 Chapman, S. C., et al. 2000, *MNRAS*, 319, 318
 Chapman, S. C., et al. 2010, *MNRAS*, 409, L13
 Chary, R., & Elbaz, D. 2001, *ApJ*, 556, 562
 Clements, D. L., Dunne, L., & Eales, S. 2010, *MNRAS*, 403, 274
 Coppin, K., et al. 2008, *MNRAS*, 384, 1597
 Cox, T. J., Dutta, S. N., Matteo, T. D., Hernquist, L., Hopkins, P. F., Robertson, B., & Springel, V. 2006a, *ApJ*, 650, 791
 Cox, T. J., Jonsson, P., Primack, J. R., & Somerville, R. S. 2006b, *MNRAS*, 373, 1013
 Cox, T. J., Jonsson, P., Somerville, R. S., Primack, J. R., & Dekel, A. 2008, *MNRAS*, 384, 386
 Daddi, E., Dannerbauer, H., Krips, M., Walter, F., Dickinson, M., Elbaz, D., & Morrison, G. E. 2009a, *ApJ*, 695, L176

- Daddi, E., et al. 2005, *ApJ*, 631, L13
—, 2007, *ApJ*, 670, 156
—, 2009b, *ApJ*, 694, 1517
—, 2010, *ApJ*, 713, 686
- Dale, D. A., & Helou, G. 2002, *ApJ*, 576, 159
- Dale, D. A., Helou, G., Contursi, A., Silberman, N. A., & Kolhatkar, S. 2001, *ApJ*, 549, 215
- Dale, D. A., et al. 2007, *ApJ*, 655, 863
- Dannerbauer, H., Daddi, E., Riechers, D. A., Walter, F., Carilli, C. L., Dickinson, M., Elbaz, D., & Morrison, G. E. 2009, *ApJ*, 698, L178
- Dannerbauer, H., et al. 2010, *ApJ*, 720, L144
- Davé, R., Finlator, K., Oppenheimer, B. D., Fardal, M., Katz, N., Kereš, D., & Weinberg, D. H. 2010, *MNRAS*, 404, 1355
- Dekel, A., et al. 2009, *Nature*, 457, 451
- Downes, D., & Solomon, P. M. 1998, *ApJ*, 507, 615
- Draine, B. T., & Li, A. 2007, *ApJ*, 657, 810
- Dunne, L., & Eales, S. A. 2001, *MNRAS*, 327, 697
- Dunne, L., Eales, S. A., & Edmunds, M. G. 2003, *MNRAS*, 341, 589
- Dwek, E. 1998, *ApJ*, 501, 643
- Eales, S., Lilly, S., Gear, W., Dunne, L., Bond, J. R., Hammer, F., Fèvre, O. L., & Crampton, D. 1999, *ApJ*, 515, 518
- Edmunds, M. G., & Eales, S. A. 1998, *MNRAS*, 299, L29
- Engel, H., et al. 2010, arXiv:1009.2495
- Erb, D. K., Steidel, C. C., Shapley, A. E., Pettini, M., Reddy, N. A., & Adelberger, K. L. 2006, *ApJ*, 646, 107
- Fontanot, F., & Monaco, P. 2010, *MNRAS*, 405, 705
- Fontanot, F., Monaco, P., Silva, L., & Grazian, A. 2007, *MNRAS*, 382, 903
- Genzel, R., Baker, A. J., Tacconi, L. J., Lutz, D., Cox, P., Guilloteau, S., & Omont, A. 2003, *ApJ*, 584, 633
- Gingold, R. A., & Monaghan, J. J. 1977, *MNRAS*, 181, 375
- Gonzalez, J. E., Lacey, C. G., Baugh, C. M., & Frenk, C. S. 2010, arXiv:1006.0230
- Granato, G. L., De Zotti, G., Silva, L., Bressan, A., & Danese, L. 2004, *ApJ*, 600, 580
- Greve, T. R., Pope, A., Scott, D., Ivison, R. J., Borys, C., Conselice, C. J., & Bertoldi, F. 2008, *MNRAS*, 389, 1489
- Greve, T. R., et al. 2005, *MNRAS*, 359, 1165
- Groves, B., Dopita, M. A., Sutherland, R. S., Kewley, L. J., Fischera, J., Leitherer, C., Brandl, B., & van Breugel, W. 2008, *ApJS*, 176, 438
- Hainline, L. J., Blain, A. W., Smail, I., Alexander, D. M., Armus, L., Chapman, S. C., & Ivison, R. J. 2010, arXiv:1006.0238
- Hayward, C. C., Narayanan, D., Jonsson, P., Cox, T. J., Kereš, D., Hopkins, P. F., & Hernquist, L. 2010, arXiv:1008.4584
- Hernquist, L. 1990, *ApJ*, 356, 359
- Hernquist, L., & Katz, N. 1989, *ApJS*, 70, 419
- Hobson, M. P., & Padman, R. 1993, *MNRAS*, 264, L161
- Holland, W. S., et al. 1999, *MNRAS*, 303, 659
- Hopkins, P. F., Cox, T. J., Dutta, S. N., Hernquist, L., Kormendy, J., & Lauer, T. R. 2009a, *ApJS*, 181, 135
- Hopkins, P. F., Cox, T. J., Kereš, D., & Hernquist, L. 2008a, *ApJS*, 175, 390
- Hopkins, P. F., Cox, T. J., Younger, J. D., & Hernquist, L. 2009b, *ApJ*, 691, 1168
- Hopkins, P. F., & Hernquist, L. 2010, *MNRAS*, 402, 985
- Hopkins, P. F., Hernquist, L., Cox, T. J., Di Matteo, T., Robertson, B., & Springel, V. 2006a, *ApJS*, 163, 1
- Hopkins, P. F., Hernquist, L., Cox, T. J., Dutta, S. N., & Rothberg, B. 2008b, *ApJ*, 679, 156
- Hopkins, P. F., Hernquist, L., Cox, T. J., & Kereš, D. 2008c, *ApJS*, 175, 356
- Hopkins, P. F., Hernquist, L., Cox, T. J., Robertson, B., & Springel, V. 2006b, *ApJS*, 163, 50
- Hopkins, P. F., Lauer, T. R., Cox, T. J., Hernquist, L., & Kormendy, J. 2009c, *ApJS*, 181, 486
- Hopkins, P. F., Richards, G. T., & Hernquist, L. 2007, *ApJ*, 654, 731
- Hopkins, P. F., Somerville, R. S., Hernquist, L., Cox, T. J., Robertson, B., & Li, Y. 2006c, *ApJ*, 652, 864
- Hopkins, P. F., Younger, J. D., Hayward, C. C., Narayanan, D., & Hernquist, L. 2010, *MNRAS*, 402, 1693
- Hopkins, P. F., et al. 2009d, *MNRAS*, 397, 802
- Hughes, D. H., et al. 1998, *Nature*, 394, 241
- Hwang, H. S., et al. 2010, *MNRAS*, 409, 75
- Iono, D., et al. 2009, *ApJ*, 695, 1537
- Ivison, R. J., et al. 2002, *MNRAS*, 337, 1
—, 2007, *MNRAS*, 380, 199
- James, A., Dunne, L., Eales, S., & Edmunds, M. G. 2002, *MNRAS*, 335, 753
- Jonsson, P. 2006, *MNRAS*, 372, 2
- Jonsson, P., Cox, T. J., Primack, J. R., & Somerville, R. S. 2006, *ApJ*, 637, 255
- Jonsson, P., Groves, B. A., & Cox, T. J. 2010, *MNRAS*, 403, 17
- Jonsson, P., & Primack, J. R. 2010, *NewA*, 15, 509
- Juvela, M. 2005, *A&A*, 440, 531
- Katz, N., Weinberg, D. H., & Hernquist, L. 1996, *ApJS*, 105, 19
- Kennicutt, R. C. 1998a, *ApJ*, 498, 541
—, 1998b, *ARA&A*, 36, 189
- Kennicutt, Jr., R. C., et al. 2003, *PASP*, 115, 928
- Kereš, D., Katz, N., Fardal, M., Davé, R., & Weinberg, D. H. 2009, *MNRAS*, 395, 160
- Kereš, D., Katz, N., Weinberg, D. H., & Davé, R. 2005, *MNRAS*, 363, 2
- Knudsen, K. K., Kneib, J.-P., Richard, J., Petitpas, G., & Egami, E. 2010, *ApJ*, 709, 210
- Kormendy, J., Fisher, D. B., Cornell, M. E., & Bender, R. 2009, *ApJS*, 182, 216
- Kovács, A., Chapman, S. C., Dowell, C. D., Blain, A. W., Ivison, R. J., Smail, I., & Phillips, T. G. 2006, *ApJ*, 650, 592
- Kovács, A., et al. 2010, *ApJ*, 717, 29
- Kroupa, P. 2001, *MNRAS*, 322, 231
- Krumholz, M. R., & Thompson, T. A. 2007, *ApJ*, 669, 289
- Leitherer, C., et al. 1999, *ApJS*, 123, 3
- Lisenfeld, U., Isaak, K. G., & Hills, R. 2000, *MNRAS*, 312, 433
- Lo Faro, B., Monaco, P., Vanzella, E., Fontanot, F., Silva, L., & Cristiani, S. 2009, *MNRAS*, 399, 827
- Lonsdale, C. J., Farrah, D., & Smith, H. E. 2006, *Ultraluminous Infrared Galaxies*, ed. Mason, J. W. (Springer Verlag), 285
- Lucy, L. B. 1977, *AJ*, 82, 1013
- Lupu, R. E., et al. 2010, arXiv:1009.5983
- Magdis, G. E., et al. 2010, *MNRAS*, 409, 22
- Magnelli, B., et al. 2010, *A&A*, 518, L28+
- Matteo, T. D., Springel, V., & Hernquist, L. 2005, *Nature*, 433, 604
- Menéndez-Delmestre, K., et al. 2007, *ApJ*, 655, L65
—, 2009, *ApJ*, 699, 667
- Michałowski, M., Hjorth, J., & Watson, D. 2010a, *A&A*, 514, A67
- Michałowski, M. J., Watson, D., & Hjorth, J. 2010b, *ApJ*, 712, 942
- Mihos, J. C., & Hernquist, L. 1994, *ApJ*, 437, L47
—, 1996, *ApJ*, 464, 641
- Narayanan, D., Cox, T. J., Hayward, C. C., & Hernquist, L. 2010a, arXiv:1005.3020
- Narayanan, D., Cox, T. J., Hayward, C. C., Younger, J. D., & Hernquist, L. 2009, *MNRAS*, 400, 1919
- Narayanan, D., Cox, T. J., Shirley, Y., Davé, R., Hernquist, L., & Walker, C. K. 2008a, *ApJ*, 684, 996
- Narayanan, D., Hayward, C. C., Cox, T. J., Hernquist, L., Jonsson, P., Younger, J. D., & Groves, B. 2010b, *MNRAS*, 401, 1613 (N10)
- Narayanan, D., et al. 2008b, *ApJS*, 174, 13
—, 2010c, *MNRAS*, 407, 1701
- Neri, R., et al. 2003, *ApJ*, 597, L113
- Noeske, K. G., et al. 2007a, *ApJ*, 660, L47
—, 2007b, *ApJ*, 660, L43
- Peacock, J. A., et al. 2000, *MNRAS*, 318, 535
- Pope, A., et al. 2006, *MNRAS*, 370
—, 2008, *ApJ*, 675, 1171
- Rex, M., et al. 2010, *A&A*, 518, L13+
- Robertson, B., Bullock, J. S., Cox, T. J., Di Matteo, T., Hernquist, L., Springel, V., & Yoshida, N. 2006a, *ApJ*, 645, 986
- Robertson, B., Hernquist, L., Cox, T. J., Matteo, T. D., Hopkins, P. F., Martini, P., & Springel, V. 2006b, *ApJ*, 641, 90
- Rothberg, B., & Fischer, J. 2010, *ApJ*, 712, 318
- Rothberg, B., & Joseph, R. D. 2004, *AJ*, 128, 2098
- Sakamoto, K., Scoville, N. Z., Yun, M. S., Crosas, M., Genzel, R., & Tacconi, L. J. 1999, *ApJ*, 514, 68
- Sakamoto, K., et al. 2008, *ApJ*, 684, 957
- Sanders, D. B., & Mirabel, I. F. 1996, *ARA&A*, 34, 749
- Schinnerer, E., et al. 2008, *ApJ*, 689, L5
- Scott, S. E., et al. 2002, *MNRAS*, 331, 817
- Scoville, N. Z., Sargent, A. I., Sanders, D. B., & Soifer, B. T. 1991, *ApJ*, 366, L5
- Smail, I., Chapman, S. C., Blain, A. W., & Ivison, R. J. 2004, *ApJ*, 616, 71
- Smail, I., Ivison, R. J., & Blain, A. W. 1997, *ApJ*, 490, L5
- Somerville, R. S., Hopkins, P. F., Cox, T. J., Robertson, B. E., & Hernquist, L. 2008, *MNRAS*, 391, 481
- Springel, V. 2005, *MNRAS*, 364, 1105
- Springel, V., & Hernquist, L. 2002, *MNRAS*, 333, 649
—, 2003, *MNRAS*, 339, 289
- Springel, V., Matteo, T. D., & Hernquist, L. 2005, *MNRAS*, 361, 776
- Springel, V., Yoshida, N., & White, S. D. M. 2001, *NewA*, 6, 79
- Swinbank, A. M., Smail, I., Chapman, S. C., Blain, A. W., Ivison, R. J., & Keel, W. C. 2004, *ApJ*, 617, 64
- Swinbank, A. M., et al. 2008, *MNRAS*, 391, 420
- Tacconi, L. J., et al. 2006, *ApJ*, 640, 228
—, 2008, *ApJ*, 680, 246
—, 2010, *Nature*, 463, 781
- Valiante, E., et al. 2007, *ApJ*, 660, 1060

van Kampen, E., et al. 2005, MNRAS, 359, 469
 Városi, F., & Dwek, E. 1999, ApJ, 523, 265
 Wang, W., Cowie, L. L., Barger, A. J., & Williams, J. P. 2010, arXiv:1012.1071
 Webb, T. M., et al. 2003, ApJ, 582, 6
 Weingartner, J. C., & Draine, B. T. 2001, ApJ, 548, 296
 Wilson, G. W., et al. 2008, MNRAS, 386, 807
 Witt, A. N., & Gordon, K. D. 1996, ApJ, 463, 681
 Wright, E. L. 2006, PASP, 118, 1711
 Wuyts, S., Cox, T. J., Hayward, C. C., Franx, M., Hernquist, L., Hopkins, P. F., Jonsson, P., & van Dokkum, P. G. 2010, ApJ, 722, 1666

Wuyts, S., et al. 2009, ApJ, 700, 799
 Younger, J. D., Hayward, C. C., Narayanan, D., Cox, T. J., Hernquist, L., & Jonsson, P. 2009a, MNRAS, 396, L66
 Younger, J. D., et al. 2007, ApJ, 671, 1531
 —. 2008, ApJ, 688, 59
 —. 2009b, MNRAS, 394, 1685
 —. 2009c, ApJ, 704, 803
 —. 2010, MNRAS, 407, 1268

APPENDIX

DERIVATION OF THE RELATIONS GIVEN IN §3.2.1

Here we derive the relations for submm flux density as a function of dust bolometric luminosity L_d and dust mass M_d (Equation 4) and SFR and M_d (Equation 3) for an optically thin modified blackbody. One can model galaxy SEDs with more complex models (e.g., Dale et al. 2001; Dale & Helou 2002; Chakrabarti & McKee 2005, 2008; Kovács et al. 2010), but for the sake of simplicity and because the optically thin modified blackbody is commonly used for SED fitting we only consider an optically thin modified blackbody here. Consider a mass M_d of dust with temperature T_d . Assuming the dust is optically thin at rest-frame frequency ν_r , the luminosity density emitted by the dust at that frequency is

$$L_{\nu_r} = 4\pi\kappa_{\nu_r}M_dB_{\nu_r}(T_d), \quad (\text{A1})$$

where κ_{ν_r} is the dust opacity ($\text{m}^2 \text{kg}^{-1}$) at rest-frame frequency ν_r and $B_{\nu_r}(T_d)$ is the Planck function. We assume a power-law opacity in the IR,

$$\kappa_{\nu_r} = \kappa_0 \left(\frac{\nu_r}{\nu_0} \right)^\beta, \quad (\text{A2})$$

where κ_0 is the opacity at frequency ν_0 . Integrating Equation (A1) over ν gives the total dust luminosity,

$$L_d = \Gamma(4 + \beta)\zeta(4 + \beta)\frac{8\pi h}{c^2} \left(\frac{kT_d}{h} \right)^4 M_d\kappa_0 \left(\frac{kT_d}{h\nu_0} \right)^\beta, \quad (\text{A3})$$

where Γ and ζ are Riemann functions, h is the Planck constant, c is the speed of light, and k is the Boltzmann constant. Solving for the effective dust temperature yields

$$T_d = \frac{h}{k} \left[\frac{L_d c^2 \nu_0^\beta}{\Gamma(4 + \beta)\zeta(4 + \beta)8\pi\kappa_0 h M_d} \right]^{1/(4+\beta)}. \quad (\text{A4})$$

If we place the mass of dust at redshift z , the flux density at observed-frame frequency ν_o is

$$S_{\nu_o}(T_d) = (1 + z) \frac{L_{\nu_r}}{4\pi D_L^2} \quad (\text{A5})$$

$$= (1 + z) \frac{4\pi\kappa_{\nu_r}M_dB_{\nu_r}(T_d)}{4\pi D_L^2} \quad (\text{A6})$$

$$= (1 + z)^{\beta-3} \frac{\kappa_0 M_d}{D_A^2} \left(\frac{\nu_o}{\nu_0} \right)^\beta B_{\nu_o(1+z)}(T_d), \quad (\text{A7})$$

where we have related angular diameter distance D_A and luminosity distance D_L using $D_L = (1 + z)^2 D_A$. In the Rayleigh-Jeans limit, $B_\nu(T) = 2k\nu^2 T/c^2$, so

$$S_{\nu_o}(T_d) = (1 + z)^{\beta-1} \frac{2k\kappa_0}{c^2 D_A^2} \left(\frac{\nu_o}{\nu_0} \right)^\beta \nu_o^2 M_d T_d. \quad (\text{A8})$$

By substituting T_d from Equation (A4) into Equation (A8) we find

$$S_{\nu_o} = \frac{2h\kappa_0}{c^2 D_A^2} \nu_o^2 \left(\frac{\nu_o}{\nu_0} \right)^\beta \left(\frac{\nu_0^\beta c^2}{\Gamma(4 + \beta)\zeta(4 + \beta)8\pi\kappa_0 h} \right)^{1/(4+\beta)} (1 + z)^{\beta-1} L_d^{1/(4+\beta)} M_d^{(3+\beta)/(4+\beta)}. \quad (\text{A9})$$

For the Weingartner & Draine (2001) $R_V = 3.1$ Milky Way dust model, which we use in our RT calculations, $\beta \approx 2$ and the $850 \mu\text{m}$ opacity is $\kappa_{850} = 0.050 \text{m}^2 \text{kg}^{-1}$, consistent with the value James et al. (2002) derived from submm

observations of local galaxies, $0.07 \pm 0.02 \text{ m}^2 \text{ kg}^{-1}$, and with the results of Dunne et al. (2003). Thus the observed 850 μm flux density is

$$S_{850} = 1.5 \text{ mJy } (1+z) \left(\frac{D_A}{1 \text{ Gpc}} \right)^{-2} \left(\frac{L_d}{10^{12} L_\odot} \right)^{1/6} \left(\frac{M_d}{10^8 M_\odot} \right)^{5/6}. \quad (\text{A10})$$

The Kennicutt (1998b) SFR- L_{IR} calibration converted to a Kroupa (2001) initial mass function is

$$L_{\text{IR}} \approx L_{\text{bol}} \approx 9 \times 10^9 L_\odot (\text{SFR}/M_\odot \text{ yr}^{-1}). \quad (\text{A11})$$

This conversion assumes all starlight is absorbed by dust and the contribution from AGN and old stars is negligible; as discussed above, these assumptions are all violated at some level. (If these assumption were true, the power-law indices in Equations (1) and (2) would be identical.) However, since the above calibration is ubiquitously applied, we will give the relation that results when we use it; the relation is

$$S_{850} = 1.5 \text{ mJy } (1+z) \left(\frac{D_A}{1 \text{ Gpc}} \right)^{-2} \left(\frac{\text{SFR}}{100 M_\odot \text{ yr}^{-1}} \right)^{1/6} \left(\frac{M_d}{10^8 M_\odot} \right)^{5/6}. \quad (\text{A12})$$

Assuming $\Omega_m = 0.27$, $\Omega_\Lambda = 0.73$, and $h = 0.7$, the angular diameter distance at $z = 2$ is 1.77 Gpc (Wright 2006). Thus for $z = 2$ we recover Equation (4),

$$S_{850} = 1.4 \text{ mJy } \left(\frac{L_d}{10^{12} L_\odot} \right)^{1/6} \left(\frac{M_d}{10^8 M_\odot} \right)^{5/6}. \quad (\text{A13})$$

This should be compared to Equation (2). In terms of SFR, we get Equation (3),

$$S_{850} = 1.4 \text{ mJy } \left(\frac{\text{SFR}}{100 M_\odot \text{ yr}^{-1}} \right)^{1/6} \left(\frac{M_d}{10^8 M_\odot} \right)^{5/6}. \quad (\text{A14})$$

This should be compared to Equation (1).

Even if the underlying power-law index of the dust opacity curve is $\beta = 2$, for a distribution of dust temperatures a single-temperature modified blackbody with $\beta = 1.5$ may better fit the SED (Dunne & Eales 2001; Chakrabarti & McKee 2008). Furthermore, $\beta = 1.5$ is often assumed when fitting SEDs and determining dust masses of SMGs (e.g., Kovács et al. 2006, 2010; Coppin et al. 2008; Chapman et al. 2010), so we will provide the relations for $\beta = 1.5$ also. They are:

$$S_{850} = 1.9 \text{ mJy } (1+z)^{0.5} \left(\frac{D_A}{1 \text{ Gpc}} \right)^{-2} \left(\frac{L_d}{10^{12} L_\odot} \right)^{0.18} \left(\frac{M_d}{10^8 M_\odot} \right)^{0.82}, \quad (\text{A15})$$

and

$$S_{850} = 1.9 \text{ mJy } (1+z)^{0.5} \left(\frac{D_A}{1 \text{ Gpc}} \right)^{-2} \left(\frac{\text{SFR}}{100 M_\odot \text{ yr}^{-1}} \right)^{0.18} \left(\frac{M_d}{10^8 M_\odot} \right)^{0.82}. \quad (\text{A16})$$

For $z = 2$,

$$S_{850} = 1.0 \text{ mJy } \left(\frac{L_d}{10^{12} L_\odot} \right)^{0.18} \left(\frac{M_d}{10^8 M_\odot} \right)^{0.82}, \quad (\text{A17})$$

and

$$S_{850} = 1.0 \text{ mJy } \left(\frac{\text{SFR}}{100 M_\odot \text{ yr}^{-1}} \right)^{0.18} \left(\frac{M_d}{10^8 M_\odot} \right)^{0.82}. \quad (\text{A18})$$

The equations can be rescaled to different values of κ_0 using $S_{\nu_o} \propto \kappa_0^{(3+\beta)/(4+\beta)}$ and to different submm wavelengths using $S_{\nu_o} \propto \nu_o^{2+\beta}$ (see Equation A9).